

## **ELECTROMAGNETIC SCATTERING FROM PERIODIC ARRAYS OF TWO CIRCULAR CYLINDERS PER UNIT CELL**

T. Kushta and K. Yasumoto

Department of Computer Science and Communication Engineering  
Kyushu University  
6-10-1 Hakozaki, Higashi-ku  
Fukuoka 812-8581, Japan

**Abstract**—An efficient and accurate method to the problem of plane-wave scattering from periodic arrays of two circular-cylinders per unit cell is presented. The scattered fields are calculated using the lattice sums characterizing a periodic arrangement of scatterers and the aggregate  $T$ -matrix for the isolated two-cylinders system in free space. The cylinders may be of dielectric, perfect conductor, or their mixture with different dimensions. The numerical examples for the resonant scattering are presented with an emphasis on the application to the polarization-dependent or polarization independent narrow-band filters.

- 1. Introduction**
  - 2. Formulation of the Problem**
  - 3. Lattice Sums and  $T$ -Matrix**
    - 3.1 Lattice Sums
    - 3.2  $T$ -Matrix of Isolated Two Circular-Cylinders
  - 4. Numerical Examples**
  - 5. Conclusion**
- References**

### **1. INTRODUCTION**

The purpose of this paper is to present an efficient technique to calculate the scattered electromagnetic fields from periodic arrays consisting

of two circular-cylinders per unit cell. Such a periodical structure is very attractive to devise a novel wavelength and polarization selective components in microwave and optical wave regions, because additional degrees of freedom for controlling the scattered fields are available.

During the past few decades, various numerical techniques [1], such as integral equation methods, mode-matching methods, differential methods, and homogenization methods, have been developed to formulate the periodic boundary-value problems. Recently, a recursive  $T$ -matrix algorithm [2] was applied to a problem of scattering from a periodic array of one circular-cylinder per unit cell [3]. In this approach, each isolated cylinder has been divided into a large number of electrically small cylinders whose individual  $T$ -matrices can be well represented by the lower-order cylindrical harmonic expansion. Then the translation formulas and Floquet's theorem have been used to derive a linear system of equations for the scattered fields from the one-circular-cylinder array.

In this paper, we refine the recursive  $T$ -matrix approach [2] for the periodic array problem by using the concept of lattice sums [4] and develop an efficient numerical technique to calculate the scattered fields from a periodic array of composite cylinders per unit cell. It is shown that the scattered fields from such an array can be expressed in terms of the lattice sums and the aggregate  $T$ -matrix for the composite-cylinders system in isolation. The lattice sums characterize uniquely the periodic arrangement of scatterers and are independent of the polarization of incident wave and the individual configuration of scatterers. The scattering nature of each composite-cylinders located in unit cell is described by the aggregate  $T$ -matrix. This separation in the calculation of scattered fields greatly simplifies the analytical and numerical procedure for the array problems.

The lattice sums [4], are given by a semi-infinite series of Hankel functions. From the point of view of numerical computation, a substantial difficulty in the use of the lattice sums has been in a very slow convergence of the series. To overcome the difficulty, we employ here an integral form [5] of the lattice sums which can be accurately and efficiently evaluated using a simple scheme of numerical integration. The proposed technique is applied to the analysis of two-dimensional scattering by the periodic array of two circular-cylinders which may be of dielectric, conductor or their mixture with different dimensions. The numerical examples demonstrate a variety of interesting resonance

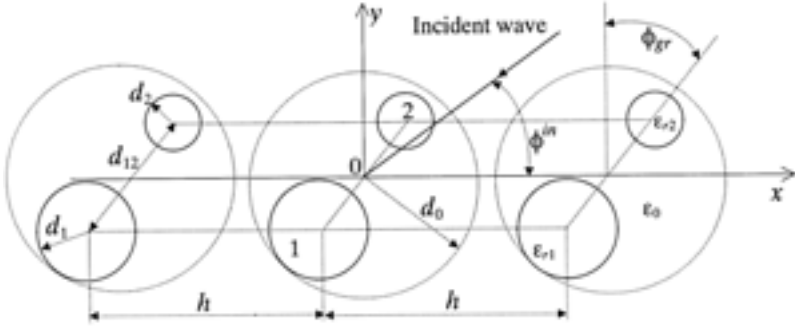


**Figure 1.** Geometry of a periodic array of two circular-cylinders per unit cell.

profiles in the scattered fields which are not realized by the arrays of one circular-cylinder per unit cell. The time dependence of the fields is assumed to be  $\exp(-i\omega t)$  and omitted throughout the paper.

## 2. FORMULATION OF THE PROBLEM

An array composed of two circular-cylinders per unit cell is situated in a background medium with a permittivity  $\varepsilon_0$  and permeability  $\mu_0$  as shown in Fig. 1. The radius, permittivity, and permeability of each cylinder are  $(d_1, \varepsilon_0\varepsilon_{r1}, \mu_0)$  and  $(d_2, \varepsilon_0\varepsilon_{r2}, \mu_0)$ , respectively. The centers of two cylinders are separated by  $d_{12}$  and the line connecting two centers makes an angle  $\phi_{gr}$  with the  $y$ -axis. The array is periodic in the  $x$ -direction with a period  $h$  and is uniform in the  $z$ -direction. The origin of the coordinate for  $l$ -th cell is chosen at  $x = lh$  and  $y = 0$ , and the local polar coordinate system is denoted by  $\rho_l = [(x - lh)^2 + y^2]^{1/2}$  and  $\cos \phi_l = (x - lh)/\rho_l$ . We consider a two-dimensional scattering problem for a plane wave impinging at an angle  $\phi^{in}$  with respect to the  $x$ -axis. The electric field  $E_z$  in the  $TM$ -wave problem and the magnetic field  $H_z$  in the  $TE$ -wave problem are described in terms of a scalar wave function  $\Psi(x, y)$ . Let  $\Psi^{in}(x, y)$  be the incident field with unit amplitude. Then  $\Psi^{in}(x, y)$  is expressed in the zeroth polar coordinate system  $(\rho_0, \phi_0)$  as follows:

$$\Psi^{in}(x, y) = \mathbf{P}_0^T \cdot \mathbf{a}^{in} \quad (1)$$

with

$$\mathbf{P}_0 = [J_n(k_0\rho_0)e^{in\phi_0}] \quad (2)$$

$$\mathbf{a}^{in} = [(-i)^n e^{-in\phi^{in}}] \quad (3)$$

where  $k_0 = 2\pi/\lambda_0$ ,  $\lambda_0$  is the wavelength in background medium,  $J_n$  is the Bessel function of the  $n$ -th order,  $\mathbf{P}_0$  and  $\mathbf{a}^{in}$  are defined as column vectors, and the superscript  $T$  denotes the transpose of the indicated vector.

We assume that the geometrical configuration of two cylinders satisfies the relation

$$d_0 \leq h/2 \quad (4)$$

where  $d_0$  is the radius of a fictitious circular cylinder which is centered at the origin of the coordinates and encircles two cylinders in unit cell as shown in Fig. 1. Then the scattered field  $\Psi^{sc}(x, y)$  outside the fictitious cylinders is expressed as an infinite sum of cylindrical harmonics outgoing from the origin in each cell. Using Floquet's theorem,  $\Psi^{sc}(x, y)$  is rewritten as follows:

$$\Psi^{sc}(x, y) = \sum_{l=-\infty}^{\infty} \mathbf{Q}_l^T \cdot \mathbf{a}_0^{sc} e^{-ilk_0 h \cos \phi^{in}} \quad (5)$$

with

$$\mathbf{Q}_l = [H_n^{(1)}(k_0 \rho_l) e^{in\phi_l}] \quad (6)$$

where  $H_n^{(1)}$  is the  $n$ -th order Hankel function of the first kind, and  $\mathbf{a}_0^{sc}$  denotes a column vector whose elements represent unknown amplitudes of the scattered field from the cylinders in the zeroth cell.

The recursive  $T$ -matrix algorithm [3] is used to determine the unknown scattering amplitude  $\mathbf{a}_0^{sc}$ . When the observation point  $(x, y)$  is located within  $\rho_0 = \sqrt{x^2 + y^2} < h$ ,  $\mathbf{Q}_l$  is expanded using the addition theorem of Hankel functions as follows:

$$\mathbf{Q}_l^T = \mathbf{Q}_0^T \cdot \bar{\bar{\xi}}_l \quad (l \neq 0) \quad (7)$$

where  $\bar{\bar{\xi}}_l$  is a matrix whose elements are given by

$$\xi_{l,mn} = H_{n-m}^{(1)}(k_0 lh). \quad (8)$$

Using Eqs. (1) and (5) with Eq. (7), the total field outside the fictitious circular-cylinders with  $\rho_l = d_0$  can be rewritten as follows:

$$\Psi(x, y) = \mathbf{P}_0^T \cdot [\mathbf{a}^{in} + \bar{\bar{L}} \cdot \mathbf{a}_0^{sc}] + \mathbf{Q}_0^T \cdot \mathbf{a}_0^{sc} \quad (9)$$

where  $\overline{\overline{\mathbf{L}}}$  is a square matrix whose elements are defined as

$$L_{mn} = S_{m-n}(k_0h, \phi^{in}) \quad (10)$$

$$\begin{aligned} S_n(k_0h, \phi^{in}) &= \sum_{l=1}^{\infty} H_n^1(lk_0h) e^{-ilk_0h \cos \phi^{in}} \\ &+ (-1)^n \sum_{l=1}^{\infty} H_n^1(lk_0h) e^{ilk_0h \cos \phi^{in}}. \end{aligned} \quad (11)$$

The semi-infinite sum  $S_n(k_0h, \phi^{in})$  Of the  $n$ -th order Hankel function is usually referred to [4] as the lattice sum of the  $n$ -th order. The first term in the right hand side of Eq. (9) may be viewed as an incident field impinging on the zeroth cell, whereas the second term is the scattered field from the two circular-cylinders located in the zeroth cell. Then the scattering amplitude  $\mathbf{a}_0^{sc}$  satisfies the relation

$$\mathbf{a}_0^{sc} = \overline{\overline{\mathbf{T}}} \cdot [\mathbf{a}^{in} + \overline{\overline{\mathbf{L}}} \cdot \mathbf{a}^{sc}] \quad (12)$$

where  $\overline{\overline{\mathbf{T}}}$  represents the aggregate  $T$ -matrix for the two circular-cylinders system in isolation. Solving Eq. (12),  $\mathbf{a}_0^{sc}$  is determined as follows:

$$\mathbf{a}_0^{sc} = (\overline{\overline{\mathbf{I}}} - \overline{\overline{\mathbf{T}}} \cdot \overline{\overline{\mathbf{L}}})^{-1} \cdot \overline{\overline{\mathbf{T}}} \cdot \mathbf{a}^{in} \quad (13)$$

where  $\overline{\overline{\mathbf{I}}}$  is the unit matrix. Equation (13) reveals that the scattered field from the array of two circular-cylinders is expressed in terms of the aggregate  $T$ -matrix for the isolated two circular-cylinders and the lattice sums characterizing the periodic arrangement of scatterers.

Noting that the expansion (7) is valid only for  $\rho_0 = \sqrt{x^2 + y^2} < h$ , Eq. (9) with the substitution of Eq. (13) can not be applied when the observation point  $(x, y)$  is located far from the zeroth cell. To derive the reflection and transmission coefficients of the array plane, Eq. (5) is rewritten in terms of the Floquet mode. Using the recurrence formula and Fourier integral representation for Hankel functions, after several manipulations, the reflected field  $\Psi^r(x, y)$  in the domain  $y > 0$  and the transmitted field  $\Psi^t(x, y)$  in the domain  $y < 0$  are obtained as follows:

$$\Psi^r(x, y) = \sum_{\nu=-\infty}^{\infty} \mathbf{p}_{\nu}^T \cdot \mathbf{a}_0^{sc} e^{i(k_{x\nu}x + k_{\nu}y)} \quad (14)$$

$$\Psi^t(x, y) = \sum_{\nu=-\infty}^{\infty} (\delta_{l0} + \mathbf{q}_\nu^T \cdot \mathbf{a}_0^{sc}) e^{i(k_{x\nu}x - k_\nu y)} \quad (15)$$

with

$$\mathbf{p}_\nu = \begin{bmatrix} \frac{2(-i)^m(k_{x\nu} + ik_\nu)^m}{hk_\nu k_0^m} & (m \geq 0) \\ \frac{2i^{|m|}(k_{x\nu} - ik_\nu)^{|m|}}{hk_\nu k_0^{|m|}} & (m < 0) \end{bmatrix} \quad (16)$$

$$\mathbf{q}_\nu = \begin{bmatrix} \frac{2(-i)^m(k_{x\nu} - ik_\nu)^m}{hk_\nu k_0^m} & (m \geq 0) \\ \frac{2i^{|m|}(k_{x\nu} + ik_\nu)^{|m|}}{hk_\nu k_0^{|m|}} & (m < 0) \end{bmatrix} \quad (17)$$

where  $k_{x\nu} = -k_0 \cos \phi^{in} + 2\nu\pi/h$ ,  $k_\nu = \sqrt{k_0^2 - k_{x\nu}^2}$ , and  $\delta_{\nu 0}$  is Kronecker's delta. Note that the first term in the right hand side of Eq. (15) indicates the incident field in the domain  $y < 0$ . The power reflection coefficient  $R_\nu$ , and the power transmission coefficient  $T_\nu$  for the  $\nu$ -th propagating mode with  $k_\nu > 0$  are given as

$$R_\nu = \frac{k_\nu}{k_0 \sin \phi^{in}} |\mathbf{p}_\nu^T \cdot \mathbf{a}_0^{sc}|^2 \quad (18)$$

$$T_\nu = \frac{k_\nu}{k_0 \sin \phi^{in}} |\delta_{l0} + \mathbf{q}_\nu^T \cdot \mathbf{a}_0^{sc}|^2. \quad (19)$$

### 3. LATTICE SUMS AND T-MATRIX

#### 3.1 Lattice Sums

The lattice sums defined by Eq. (11) are independent of the polarization of the incident wave and the individual configuration of cylinders. The lattice sums calculated once can be commonly used for the analysis of scattered *TM* and *TE* waves from arrays of any cylindrical objects. This is a main advantage of using the lattice sums. Since the direct sum in Eq. (11) converges very slowly, we employ here an integral form [5] of the lattice sums as follows:

$$\begin{aligned} \sum_{l=1}^{\infty} H_n^{(1)}(lk_0 h) e^{\mp i m k_0 h \cos \phi^{in}} &= \frac{(-1)^n}{\pi} e^{-i(\frac{\pi}{4} \pm k_0 h \cos \phi^{in})} \\ &\times \int_0^a [G_n(\tau) + G_n(-\tau)] F(\tau; k_0 h \mp \cos \phi^{in}) d\tau \quad (20) \end{aligned}$$

with

$$G_n(\tau) = \left( \tau + i\sqrt{1-\tau^2} \right)^n \quad (21)$$

$$F(\tau; k_0 h, \mp \cos \phi^{in}) = \frac{e^{ik_0 h \sqrt{1-\tau^2}}}{\sqrt{1-\tau^2} \left[ 1 - e^{ik_0 h (\sqrt{1-\tau^2} \mp \cos \phi^{in})} \right]} \quad (22)$$

where  $\tau = (1-i)t/\sqrt{2}$  and  $a$  is a positive real number chosen so that the integration satisfies a required convergence. The integrals in Eq. (20) is calculated using a simple trapezoidal formula of numerical integration for elementary functions. The accuracy was confirmed [5] by a substantial number of numerical tests.

### 3.2 $T$ -Matrix of Isolated Two Circular-Cylinders

The  $T$ -matrix of cylindrical objects in unit cell plays another important role in the present formulation. Any analytical or numerical techniques may be employed to calculate the  $T$ -matrix. When the objects in unit cell are composed of circular cylinders, in particular, the  $T$ -matrix is obtained in closed form. Let  $\bar{\bar{T}}_{1(1)}$  and  $\bar{\bar{T}}_{2(1)}$  be the  $T$ -matrices for circular cylinders 1 and 2 when isolated each other. Applying the recursive  $T$ -matrix algorithm [2] to  $\bar{\bar{T}}_{1(1)}$  and  $\bar{\bar{T}}_{2(1)}$ , the aggregate  $T$ -matrix for two circular-cylinders per unit cell as shown in Fig. 1 is deduced as follows:

$$\bar{\bar{T}} = \bar{\bar{\beta}}_{01} \cdot \bar{\bar{T}}_1 + \bar{\bar{\beta}}_{02} \cdot \bar{\bar{T}}_2 \quad (23)$$

with

$$\bar{\bar{T}}_1 = \left[ \bar{\bar{I}} - \bar{\bar{T}}_{1(1)} \cdot \bar{\bar{\alpha}}_{12} \cdot \bar{\bar{T}}_{2(1)} \cdot \bar{\bar{\alpha}}_{21} \right]^{-1} \cdot \bar{\bar{T}}_{1(1)} \cdot \left[ \bar{\bar{\beta}}_{10} + \bar{\bar{\alpha}}_{12} \cdot \bar{\bar{T}}_{2(1)} \cdot \bar{\bar{\beta}}_{20} \right] \quad (24)$$

$$\bar{\bar{T}}_2 = \left[ \bar{\bar{I}} - \bar{\bar{T}}_{2(1)} \cdot \bar{\bar{\alpha}}_{21} \cdot \bar{\bar{T}}_{1(1)} \cdot \bar{\bar{\alpha}}_{12} \right]^{-1} \cdot \bar{\bar{T}}_{2(1)} \cdot \left[ \bar{\bar{\beta}}_{20} + \bar{\bar{\alpha}}_{21} \cdot \bar{\bar{T}}_{1(1)} \cdot \bar{\bar{\beta}}_{10} \right] \quad (25)$$

where the subscripts 0 indicates the global coordinates shown in Fig. 1, the subscripts 1 and 2 refer to the local coordinates with the origins located at the centers of cylinders 1 and 2, respectively, and  $\bar{\bar{\alpha}}_{ij}$  and  $\bar{\bar{\beta}}_{ij}$  are the translation matrices [2] for cylindrical functions between  $i$  and  $j$  coordinate systems. The two cylinders may be of dielectric, conductor, or their mixture with different dimensions. The  $T$ -matrix  $\bar{\bar{T}}_{i(1)}$  ( $i = 1, 2$ ) for the isolated circular-cylinder  $i$  is given by the following diagonal matrix for the  $TM$  and  $TE$  waves, respectively:

$$\bar{\bar{T}}_{i(1)} = [t_{i,m} \delta_{mn}] \quad (i = 1, 2) \quad (26)$$

with

$$t_{i,m}^{TM} = -\frac{\sqrt{\varepsilon_{ri}} J_m(k_0 d_i) J'_m(k_i d_i) - J_m(k_i d_i) J'_m(k_0 d_i)}{\sqrt{\varepsilon_{ri}} J'_m(k_i d_i) H_m^{(1)}(k_0 d_i) - J_m(k_i d_i) H_m^{(1)'}(k_0 d_i)} \quad (27)$$

$$t_{i,m}^{TE} = -\frac{J_m(k_0 d_i) J'_m(k_i d_i) - \sqrt{\varepsilon_{ri}} J_m(k_i d_i) J'_m(k_0 d_i)}{J'_m(k_i d_i) H_m^{(1)}(k_0 d_i) - \sqrt{\varepsilon_{ri}} J_m(k_i d_i) H_m^{(1)'}(k_0 d_i)} \quad (28)$$

where  $k_i = k_0 \sqrt{\varepsilon_{ri}}$ ,  $\varepsilon_{ri}$  and  $d_i$  are the relative permittivity and radius of the cylinder  $i$ , and  $J'_m$  and  $H_m^{(1)'}$  denote the derivatives with respect to the indicated arguments.

#### 4. NUMERICAL EXAMPLES

The proposed approach has been applied to the analysis of various periodic arrays of two circular-cylinders. We shall discuss here the numerical results for the diffraction efficiency in the reflected waves with an emphasis on the resonance profiles distinct from those in periodic arrays of one circular-cylinder. The results are shown for the wavelength range  $h/\lambda_0 < 1$  and for the normal incidence, because such a situation is essential to the use of periodic arrays as the frequency and polarization selective components. In this case, only the fundamental Floquet mode with  $\nu = 0$  becomes the propagating wave. The numerical examples in what follows are obtained with the errors in the energy conservation less than  $10^{-5}$  by truncating the cylindrical harmonic expansion at  $m = \pm 12$  to evaluate the  $T$ -matrix of each isolated cylinder.

We examine first the wavelength response in reflection coefficient of arrays composed of dielectric cylinder 1 and perfectly conducting cylinder 2. Figure 2 shows the reflection coefficient  $R_0$  of  $TM$  wave as functions of normalized wavelength  $h/\lambda_0$  for the two-cylinders array with  $d_1 = 0.3h$ ,  $d_2 = 0.15h$ ,  $d_{12} = 0.55h$ ,  $\varepsilon_{r1} = 2.0$ ,  $|\varepsilon_{r2}| = \infty$ ,  $\phi_{gr} = 90^\circ$ , and  $\phi^{in} = 90^\circ$ . For comparison, the reflection coefficients of the one-cylinder array are also plotted for a perfectly conducting cylinder and a dielectric cylinder. It is seen that the reflection characteristics are drastically changed in the two-cylinders array. When a dielectric cylinder and a perfectly conducting cylinder are situated one after the

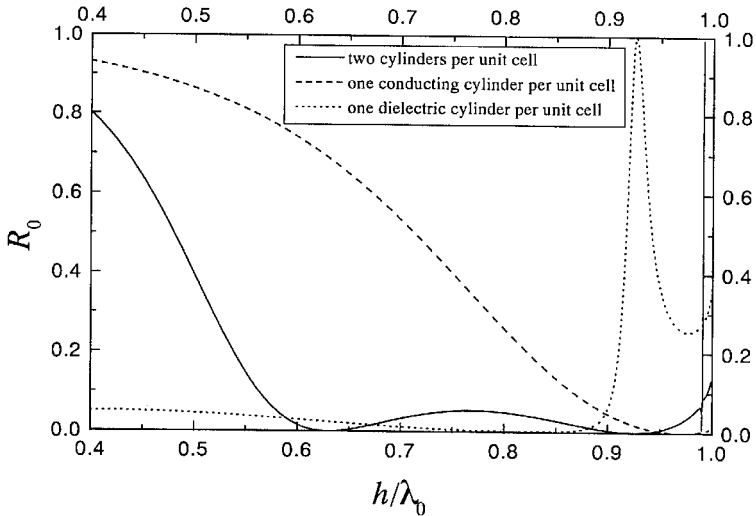


**Figure 2.** Power reflection coefficient  $R_0$  as functions of the normalized wavelength  $h/\lambda_0$  at normal incidence of  $TM$  wave for the periodic array composed of dielectric cylinder and perfectly conducting cylinder per unit cell, where  $d_1 = 0.3h$ ,  $d_2 = 0.15h$ ,  $d_{12} = 0.55h$ ,  $\varepsilon_{r1} = 2.0$ ,  $|\varepsilon_{r2}| = \infty$ ,  $\phi_{gr} = 90^\circ$ , and  $\phi^{in} = 90^\circ$ . For the array of one conducting cylinder,  $d = 0.15h$  and  $|\varepsilon_r| = \infty$ , and for the one-dielectric-cylinder array,  $d = 0.3h$  and  $\varepsilon_r = 2.0$ .

other on the same array plane, an almost zero reflectance is achieved for a wide range of wavelength over  $0.6 \leq h/\lambda_0 \leq 0.95$ . The resonance peak observed for the array of one dielectric cylinder is shifted towards larger  $h/\lambda_0$ . Figure 3 shows the similar plots for  $TE$  wave, where the values of parameters are the same as those in Fig. 2. We can see that the resonance peak observed for the array of one dielectric cylinder is shifted towards smaller  $h/\lambda_0$  under the influence of an additional cylinder of perfect conductor. The multiple scattering effect between two cylinders within unit cell makes the resonance profile sharp and reduce the side-band reflectance noticeably.

Figure 4 shows how the resonance characteristics in reflection coefficient are effected by the permittivity  $\varepsilon_{r1}$  of the dielectric cylinder of the two-cylinders array. The curves for  $\varepsilon_{r1} = 2.0$  are the same as those in Figs. 2 and 3. It is seen that a complete reflection for the  $TE$  wave is obtained at the resonance wavelength, which can be controlled by the value of relative permittivity  $\varepsilon_{r1}$  of the dielectric cylinder 1. Figures 5 to 7 show how the grating angle  $\phi_{gr}$  of two cylinders relative

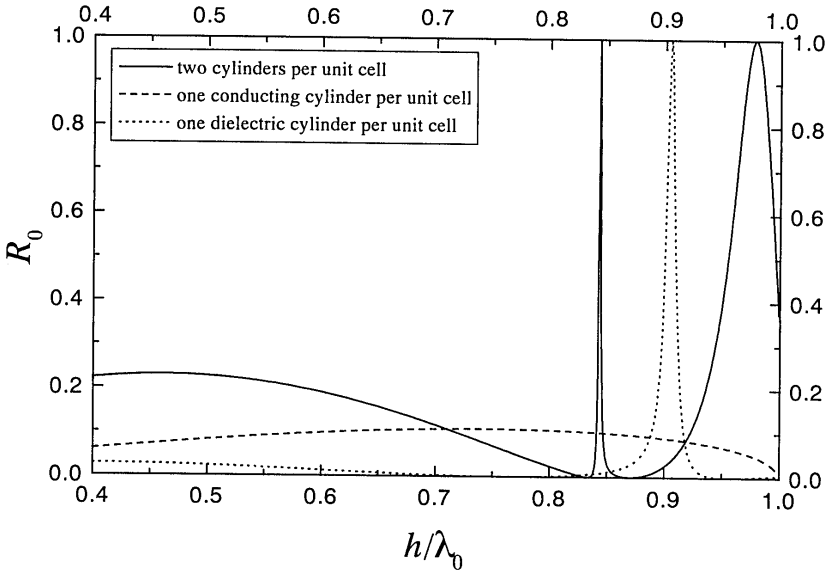


Figure 3. Same as Fig. 2 but for the normal incidence of  $TE$  wave.

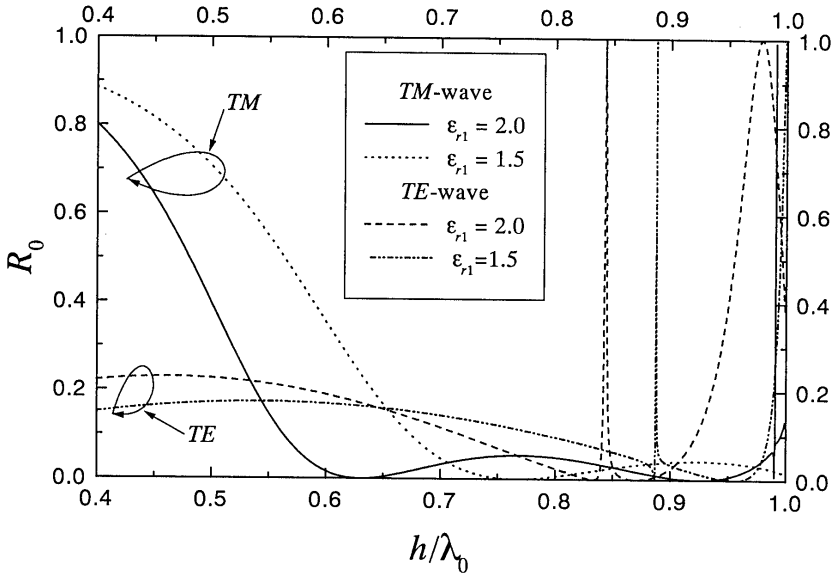
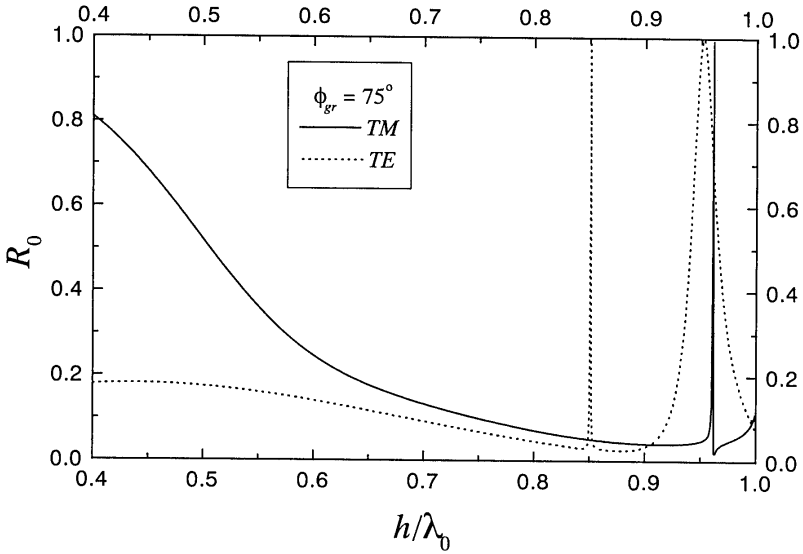
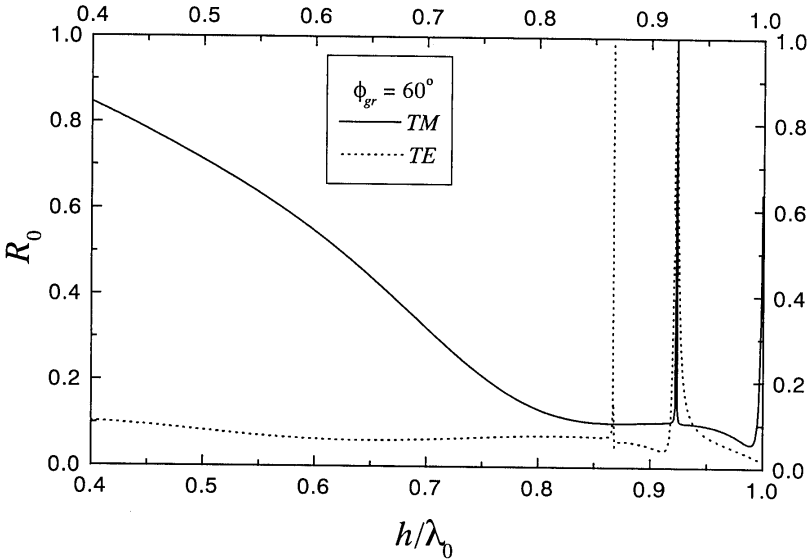


Figure 4. Power reflection coefficient  $R_0$  of the two-cylinders array for two different values of relative permittivity  $\epsilon_{r1}$  of the dielectric cylinder 1. The others are the same as those in Fig. 2.



**Figure 5.** Power reflection coefficient  $R_0$  of the two-cylinders array with the grating angle  $\phi_{gr} = 75^\circ$  for normal incidence of  $TM$  and  $TE$  waves, where  $d_1 = 0.3h$ ,  $d_2 = 0.15h$ ,  $d_{12} = 0.55h$ ,  $\varepsilon_{r1} = 2.0$ ,  $|\varepsilon_{r2}| = \infty$ , and  $\phi^{in} = 90^\circ$ .



**Figure 6.** Same as Fig. 5 but for the grating angle  $\phi_{gr} = 60^\circ$ .

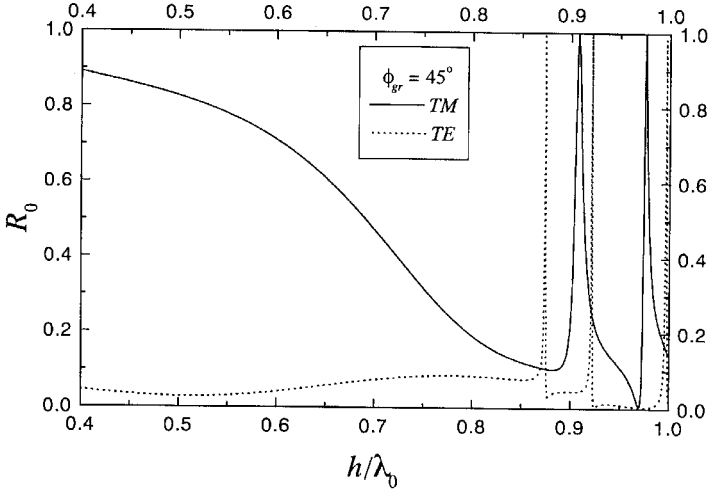


**Figure 7.** Same as Fig. 5 but for the grating angle  $\phi_{gr} = 45^\circ$ .

the array plane effects the reflection characteristics, where the other parameters are the same as those in Fig. 2. The resonance wavelengths in  $TM$  and  $TE$  waves change depending on  $\phi_{gr}$ . When the grating angle is  $60^\circ$ , we can realize an almost same resonance wavelength for both polarizations as demonstrated in Fig. 6.

We examine next the reflection characteristics of the array of two dielectric cylinders 1 and 2 per unit cell. Figure 8 shows the reflection coefficient  $R_0$  of  $TM$  wave as functions of normalized wavelength  $h/\lambda_0$  for the array with  $d_1 = 0.3h$ ,  $d_2 = 0.15h$ ,  $d_{12} = 0.55h$ ,  $\varepsilon_{r1} = 2.0$ ,  $\phi_{gr} = 90^\circ$ ,  $\phi^{in} = 90^\circ$ , and two different values of  $\varepsilon_{r2}$ . For comparison, the reflection coefficient of the array of one-dielectric-cylinder is also plotted by the solid line. The array of one-dielectric-cylinder shows a single resonance peak with a broad side-reflectance, whereas the two-cylinders array exhibits two resonance peaks with very narrow bandwidth. It is seen that the two resonance wavelengths and their relative separation are controlled by the relative permittivity  $\varepsilon_{r2}$  of the second dielectric cylinder 2. Figure 9 shows the similar plot for  $TE$  wave. Although the shift in the resonance wavelengths and the reduction of side-band reflectance are not so noticeable, we can observe the same features as in the  $TM$  wave case.

Figure 10 shows the reflection coefficient  $R_0$  of  $TM$  and  $TE$  waves for the array with  $d_1 = 0.3h$ ,  $d_2 = 0.15h$ ,  $d_{12} = 0.45h$ ,  $\varepsilon_{r1} = 2.0$ ,  $\varepsilon_{r2} = 2.25$ ,  $\phi_{gr} = 0^\circ$  and  $\phi^{in} = 90^\circ$ . In this case the array

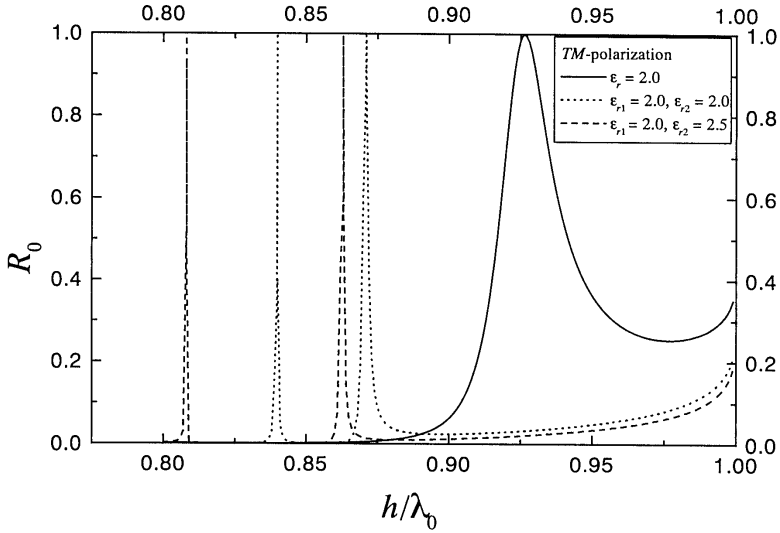


**Figure 8.** Power reflection coefficient  $R_0$  of the two-dielectric-cylinders array for normal incidence of  $TM$  wave, where  $d_1 = 0.3h$ ,  $d_2 = 0.15h$ ,  $d_{12} = 0.55h$ ,  $\varepsilon_{r1} = 2.0$ ,  $\phi_{gr} = 90^\circ$ ,  $\phi^{in} = 90^\circ$ , and  $\varepsilon_{r2} = 2.0$  or  $2.5$ . For the one-dielectric-cylinder array,  $d = 0.3h$  and  $\varepsilon_r = 2.0$ .

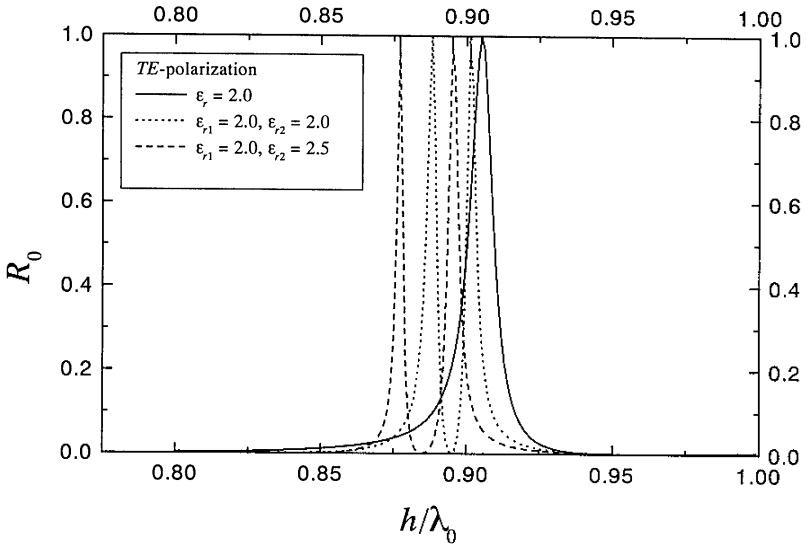


**Figure 9.** Same as Fig. 8 but for the normal incidence of  $TE$  wave.

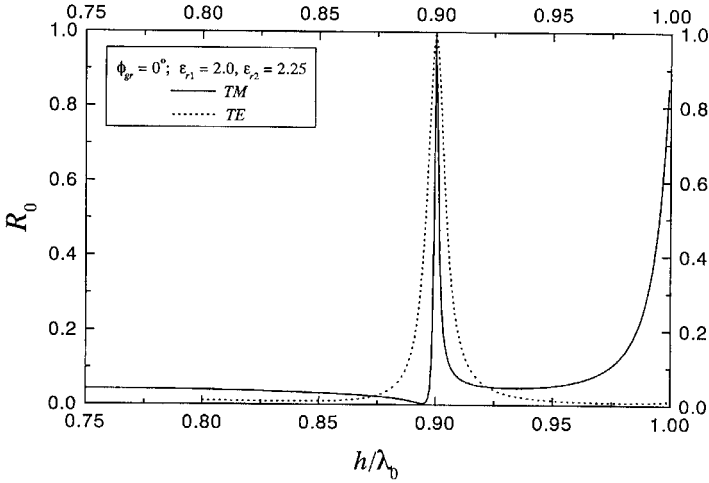


**Figure 10.** Power reflection coefficient  $R_0$  of the two-dielectric-cylinders array with the grating angle  $\phi_{gr} = 0^\circ$  for normal incidence of  $TM$  and  $TE$  waves, where  $d_1 = 0.3h$ ,  $d_2 = 0.15h$ ,  $d_{12} = 0.45h$ ,  $\epsilon_{r1} = 2.0$ ,  $\epsilon_{r2} = 2.25$ , and  $\phi^{in} = 90^\circ$ .

of two cylinders may be regarded as two-layered arrays each of which is constituted from one cylinder per unit cell. We can see that the resonance wavelengths in  $TM$  and  $TE$  waves coincide and the bandwidth of the  $TE$ -wave resonance is broader than that of the  $TM$ -wave resonance. This suggests that two-layered arrays consisting of different dielectric-cylinders may be utilized as a dual bandwidth narrow-hand filters [6] by rotating the array along its surface normal.

Figure 11 shows the reflection coefficient  $R_0$  of  $TM$  and  $TE$  waves for the array with  $d_{12} = 0.55h$ ,  $\epsilon_{r1} = \epsilon_{r2} = 2.0$ , and  $\phi_{gr} = 75^\circ$ , where the values of other parameters are the same as those in Fig. 10. When the grating angle is chosen appropriately, there appear two resonance peaks for both polarizations in the complementary wavelength region. The two resonances in  $TE$  wave have nearly same profiles, whereas those in  $TM$  wave exhibit different features. It is seen that the resonance at shorter wavelength near  $h/\lambda_0 = 0.87$  is narrow-band, but the resonance at longer wavelength near  $h/\lambda_0 = 0.85$  is broad-band. The broad-band resonance profile in  $TM$  wave can be reformed changing the value of permittivity of the second cylinder. Figure 12 shows the similar plots for  $\epsilon_{r2} = 2.5$  with other parameters same as those in Fig. 11. We can see that two resonance peaks in  $TM$  wave

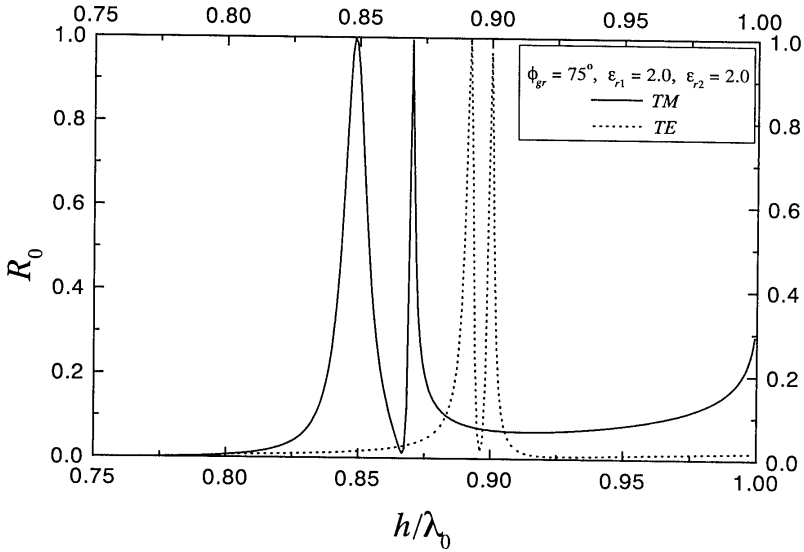


**Figure 11.** Power reflection coefficient  $R_0$  of the two-dielectric-cylinders array with the grating angle  $\phi_{gr} = 75^\circ$  for normal incidence of  $TM$  and  $TE$  waves, where  $d_1 = 0.3h$ ,  $d_2 = 0.15h$ ,  $d_{12} = 0.55h$ ,  $\epsilon_{r1} = 2.0$ ,  $\epsilon_{r2} = 2.0$ , and  $\phi^{in} = 90^\circ$ .

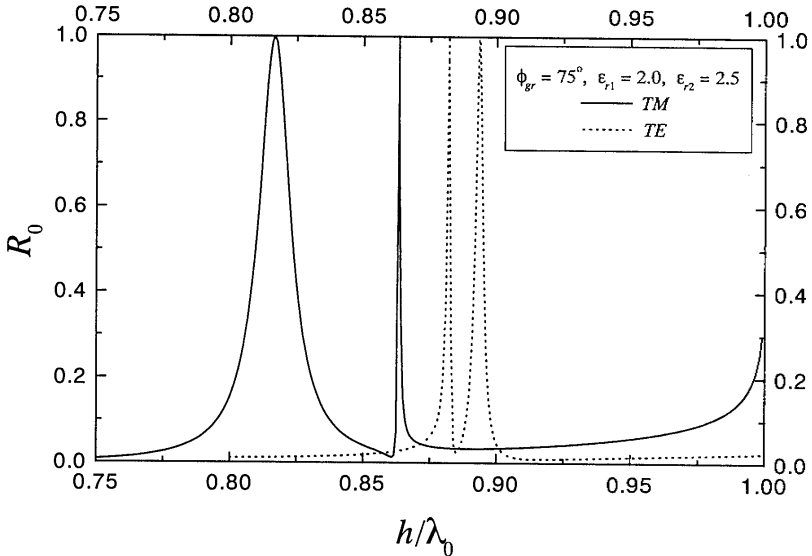


**Figure 12.** Same as Fig. 11 but  $\epsilon_{r1} = 2.0$  and  $\epsilon_{r2} = 2.5$ .

become to be well separated and a very fine broad-band resonance profile is obtained. The resonance features depicted in Fig. 12 may be used to design a polarization-dependent double-resonance filters.

## 5. CONCLUSION

An efficient and accurate technique for the problem of two-dimensional scattering from the arrays of two circular-cylinders per unit cell has been presented. The method enables us to provide a complete description of the scattered fields in terms of the lattice sums for the periodic arrangement of scatterers and the aggregate  $T$ -matrix of the two-cylinders system in isolation. This greatly simplifies the analytical and numerical procedure for the array problem. The numerical results for the resonant scattering for  $TM$  and  $TE$  polarized waves demonstrate the promising applications of two-cylinders array to a scattering of polarization-dependent or polarization-independent narrow-band filters. The extension of the present method to scattering problems for a multilayered structure of periodic arrays with  $N$  circular-cylinders per unit cell is straightforward.

## ACKNOWLEDGMENT

This work was supported in part by the Grant-in-Aid for Scientific Research (B), No. 09450155, 1999 and the Grant-in-Aid for JSPS Fellows, No. 98060, 1999 of the Ministry of Education, Science, Sports and Culture.

## REFERENCES

1. Petit, R., *Electromagnetic Theory of Gratings*, Springer-Verlag, New York, 1980.
2. Chew, W. C., *Waves and Fields in Inhomogeneous Media*, Van Nostrand Reinhold, New York, 1990.
3. Roussel, H., W. C. Chew, F. Jouvie, and W. Tabbara, "Electromagnetic scattering from dielectric and magnetic gratings of fibers — a T-matrix solution," *JEWA*, Vol. 10, No. 1, 109–127, January 1996.
4. Nicorovici, N. A. and R. C. McPhedran, "Lattice sums for off-axis electromagnetic scattering by gratings," *Phys. Rev. E*, Vol. 50, No. 4, 3143–3160, October 1994.

5. Yasumoto, K. and K. Yoshitomi, "Efficient calculation of lattice sums for freespace periodic Green's function," *IEEE Trans. Antennas Propagat.*, Vol. 47, No. 6, 1050–1055, June 1999.
6. Peng, S. and G. M. Morris, "Resonant scattering from two-dimensional gratings," *J. Opt. Soc. Am. A*, Vol. 13, No. 5, 993–1005, May 1996.